SUPPLEMENTARY MATERIAL

REFERENCES

45. Sohal, V.S., Zhang, F., Yizhar, O. & Deisseroth, K. Parvalbumin neurons and gamma rhythms enhance cortical circuit performance. *Nature* **459**, 698-702 (2009).

SUPPLEMENTARY NOTE

Statistical Analysis

All statistical tests were chosen based on normality of data and appropriateness of comparison to be analyzed by a particular approach. Data that were not normally distributed were either transformed to achieve normality, or analyzed with a test that does not assume normal distribution. Estimation of variance was performed by Bartlett's test for equal variance (for ANOVAs) or by an F test to compare variance (for unpaired t-tests). Variances were equal except when explicitly noted, below.

All error bars reported as s.e.m.

Supplementary Figure 3e. $n = 5$ for ChR2-eYFP group, $n = 5$ for L141 group, $n = 5$ for K75 group. One-way Type I ANOVA detected significant difference between the means: $F_{2,12} = 28.08$, <0.0001. ChR2-eYFP group showed significant differences with both L141 and K75 groups: $p<0.001$, Dunnett's multiple comparison tests.

Supplementary Figure 4g. $n = 8$ for fSyn-ChR2-eYFP group, $n = 5$ for intron 1+lox group, $n = 6$ for C417A group ("exon donor"), $n = 6$ for iC4A group ("intron donor), $n = 5$ for polypyrimidine group ("intron acceptor"), $n = 4$ for iC4A;polypyrimidine group, $n = 4$ for C417A;iC4A;polypyrimidine group. One-way Type I ANOVA detected significant difference between the means: $F_{6,31} = 2.590$, $p = 0.0376$. fSyn-ChR2-eYFP and iC4A showed significant differences: $p<0.05$, Dunnett's multiple comparison test.

Supplementary Figure 5c. n = 5 for ChR2 group, n = 5 for N-terminus group, n = 5 for C-terminus group. One-way type I ANOVA detected significant differences between the means $F_{2,12}$ = 10.38, <0.0001. ChR2 group was significantly different from both the N-terminus and C-terminus groups: p<0.01 for both, Dunnett's multiple comparison tests. Note that compared populations were heteroskedastic; post-hoc results remained significant when assessed with non-parametric Dunn's multiple comparison test.

Supplementary Figure 9e. n = 16 for C_{on}/F_{on}+MI-Cre+MI-Flp group, n = 20 for C_{on}/F_{on}+MI-Cre group, n = 20 for C_{on}/F_{on}+MI-Flp group. One-way type I ANOVA detected significant differences between the means $F_{2,53}$= 26.16, <0.0001. C_{on}/F_{on}+MI-Cre+MI-Flp group was significantly different from both the C_{on}/F_{on}+MI-Cre and C_{on}/F_{on}+MI-Flp groups during the light-on epoch: p<0.0001 for both, Dunnett's multiple comparison tests. C_{on}/F_{on}+MI-Cre+MI-Flp light-on was significantly different from light-off: p = 0.0005, Wilcoxon signed rank *t*-test. Note that compared populations were heteroskedastic; post-hoc results remained significant when assessed with non-parametric Dunn's multiple comparison test.

Supplementary Figure 10. Input resistance: Data were transformed (y=log(y)) to achieve normality (assessed by D'Agostino and Pearson omnibus normality test). Analysis by individual construct: One-way type 1 ANOVA detected no significant difference between the means: $F_{7,74}$ = 0.7256, p = 0.6507. Tukey's Multiple Comparison test of all pairs revealed no significant differences. n = 9 for cDIO+mCherry group, n = 10 for cDIO+MI-Cre group, n = 10 for fDIO+mCherry group, n = 11 for fDIO+MI-Flp group, n = 10 for C_{on}/F_{on}+mCherry group, n = 11 C_{on}/F_{on}+MI-Cre group, n = 11 for C_{on}/F_{on}+MI-Flp group, n = 10 for C_{on}/F_{on}+MI-Cre+MI-Flp group. Analysis grouped by ORF configuration: One-way type 1 ANOVA detected no significant difference between the means: $F_{3,78}$ = 1.597, p = 0.1969. Dunnett's post-tests comparing inactive configurations to active configuration are non-significant.

Capacitance: Analysis by individual construct: One-way type 1 ANOVA detected no significant difference between the means: $F_{7,74}$ = 1.798, p = 0.1004. Tukey's Multiple

Comparison test of all pairs revealed no significant differences. n = 9 for cDIO+mCherry group, n = 10 for cDIO+MI-Cre group, n = 10 for fDIO+mCherry group, n = 11 for fDIO+MI-Flp group, n = 10 for C_{on}/F_{on}+mCherry group, n = 11 C_{on}/F_{on}+MI-Cre group, n = 11 for C_{on}/F_{on}+MI-Flp group, n = 10 for C_{on}/F_{on}+MI-Cre+MI-Flp group. Analysis grouped by ORF configuration: One-way type 1 ANOVA detected no significant difference between the means: $F_{3,78} = 2.342$, p = 0.0796. Dunnett's post-tests comparing inactive configurations to active configuration are non-significant.

Cell counts: Chi-Squared tests of inter-condition proportions of BFP+/mCherry+ cells vs. total mCherry+ cells as counted by a blinded observer were non-significant for cDIO: χ^2 (1, N=125) = 0.2739, p = 0.6007, non-significant for fDIO: χ^2 (1, N=102) = 1.497, p = 0.2212, and significant for C_{on}/F_{on}: χ^2 (3, N=301) = 8.035, p = 0.0453. Analysis grouped by ORF configuration: One-way type 1 ANOVA detected no significant difference between the means: $F_{3,12} = 2.002$, p = 0.1675. Dunnett's post-tests comparing inactive configurations to active configuration are non-significant. Wilcoxon Signed Rank Test (comparing each inactive condition to theoretical value of "1") was non-significant.

Supplementary Figure 11b. n = 6 for ChR2-eYFP group, n = 6 for C_{on}/F_{off} group, n = 5 for 5' atg Δ gta group, n = 5 for 3' atg Δ gta group, n = 5 for 5'/3' atg Δ gta group, n = 6 for 5' atg Δ gta;3' atg Δ cta group. One-way type I ANOVA detected significant differences between the means $F_{5,27} = 8.35$, $p<0.0001$. Bonferroni's Multiple Comparison test for differences between CY and other constructs detected significant ($p<0.05$) differences between CY vs. C_{on}/F_{off} and CY vs. 5' atg Δ gta. Bonferroni's Multiple Comparison test for differences between C_{on}/F_{off} and other constructs detected significant ($p<0.05$) differences between C_{on}/F_{off} vs. 5'/3' atg Δ gta and C_{on}/F_{off} vs. 5' atg Δ gta;3' atg Δ cta group.

Mouse Genotyping protocols:

Transgene	Primers (5' -> 3')	PCR (°C)	Band Size (bp)
Cre	F: AAGAACCTGATGGACATGTTCAGGGATCG R: CCACCGTCAGTACGTGAGATATCTTTAACC	94 x 3 min 94 x 45 sec 65 x 30 sec 72 x 90 sec 30 times 72 x 10 min	550
Flp	F: GACAAGGGCAACAGCCACAGCA R: TTGCTGATGGGGTCGTAGGCGTAG	95 x 3 min 94 x 10 sec 55 x 30 sec 68 x 1 min 10 times 94 x 15 sec 55 x 30 sec 68 x 80 sec 25 times 68 x 7 min	707

Stereotactic injections

Stereotactic viral injections were carried out as previously described[45]. Briefly, mice induced and maintained on isoflurane anesthesia were placed in a stereotactic frame (Kopf Instruments) and the head leveled using bregma and lambda skull landmarks. Craniotomies were performed so as to cause minimal damage to cortical tissue using a hand drill. Injections were made using a 10μL syringe and 35g beveled needle (World Precision Instruments). 1000 nl of viral suspension was infused at a rate of 100-150 nl/min at the following coordinates (mm):

	A/P	M/L	D/V
Medial Prefrontal Cortex	+1.80	0.35	-2.85
CA1 anterior	-1.75	1.00	-1.15
CA1 medial	-2.50	1.60	-1.3
CA1 posterior	-2.80	2.00	-1.3
Dentate Gyrus	-2.5	1.6	-2.1
Nucleus Accumbens	+1.2	0.75	-4.5
Ventral Tegmental Area (dorsal)	-3.3	0.4	-4.2
Ventral Tegmental Area (ventral)	-3.3	0.4	-4.7

Supplementary Figure 1 - INTRSECT: single-component targeting of cells using multiple-feature Boolean logic

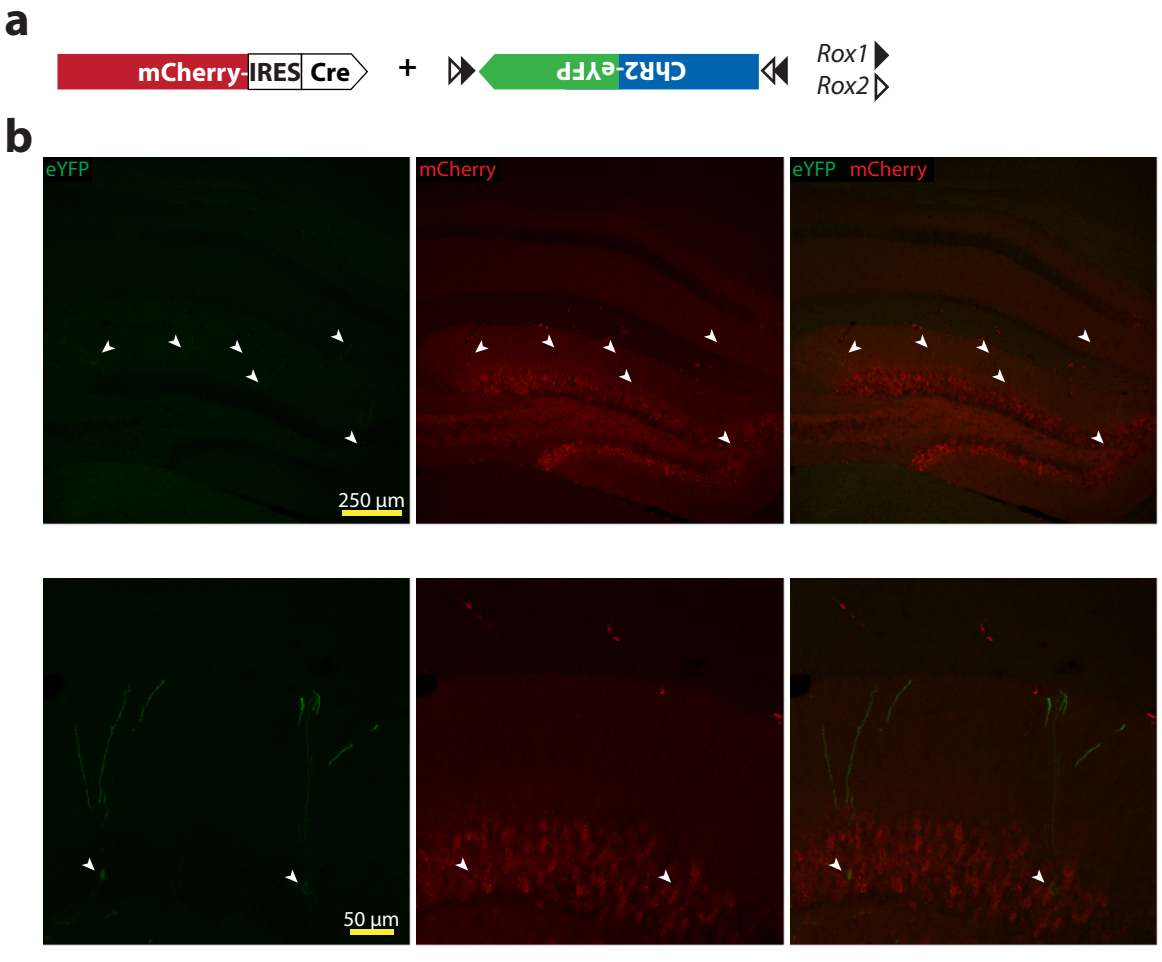

Supplementary Figure 1. ***In vivo*** **activation of dDIO by Cre recombinase. a)** Wild-type mice were co-injected with one AAV containing Cre and mCherry and a second containing Dre recombinase-dependent dDIO-ChR2-eYFP. **b)** dDIO-ChR2-eYFP activity is seen in mCherry-IRES-Cre expressing cells (arrowheads), indicating activation of dDIO-ChR2-eYFP by Cre.

Nature Methods: doi:10.1038/nmeth.2996

Supplementary Figure 2 - INTRSECT: single-component targeting of cells using multiple-feature Boolean logic

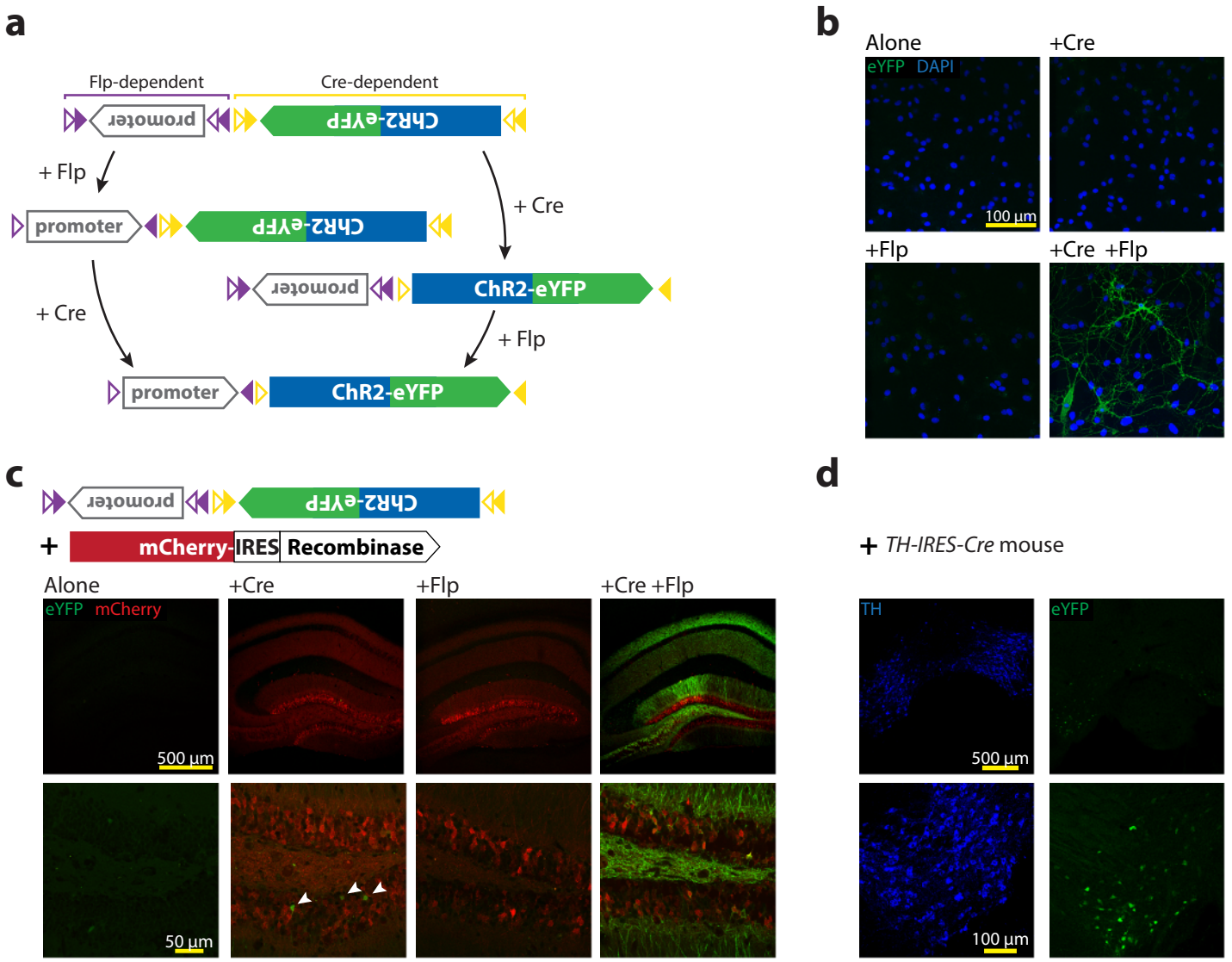

Supplementary Figure 2. Recombinase/viral strategies for intersectional genetic targeting: promoter and ORF approach. a) Schematic of independent directional control of promoter (Doublefloxed Inverted Promoter; 'DIP') and ORF (DIO) by Flp and Cre, respectively. The promoter and ORF are in the reverse orientation. Flp activity reverses the direction of the promoter, while Cre activity reverses the direction of the reading frame. The action of both Cre and Flp will position the promoter and ORF in the correct orientation. **b)** DIP/DIO-ChR2-eYFP is only expressed in cultured neurons in the presence of both Cre and Flp. **c)** To examine function of this strategy *in vivo*, DIP/DIO-ChR2-eYFP and mCherry-tagged recombinases were injected as indicated in wild type animals. Robust expression was observed in the triple-injection condition, while no expression was observed when DIP/DIO was injected alone or with Flp. Sparse cells were observed when co-injected with Cre (arrowheads). Imaging settings were individually optimized for each image. **d)** Further examination of this leak was investigated by injection of DIP/DIO-ChR2-eYFP into the VTA of *TH-IRES-Cre* animals. Extensive expression throughout the VTA was observed, validating observed leak in dual DIP/DIO + Cre injection in **c**.

Supplementary Figure 3 - INTRSECT: single-component targeting of cells using multiple-feature Boolean logic

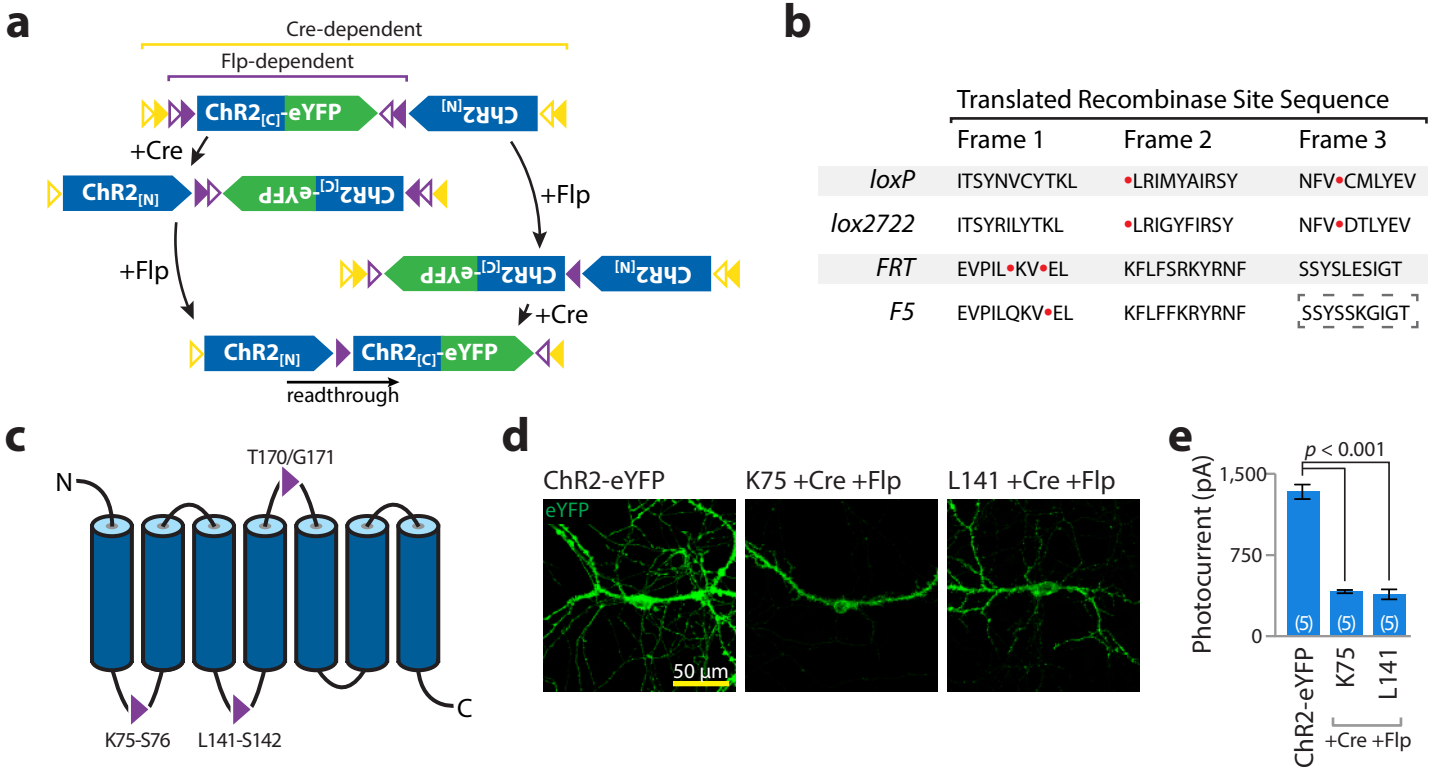

Supplementary Figure 3. Recombinase/viral strategies for intersectional genetic targeting: nested recombinase approach. a) Schematic of independent directional control of complete ORF and N-terminal of ChR2-eYFP with nested Cre and Flp DIO. The action of Cre and Flp position the entire reading frame in the correct orientation, leaving a single recombinase recognition site in-frame within the coding sequence of ChR2. **b)** Translation of four recombinase recognition sites in three reading frames. Red dots indicate STOP codons, dashed box indicates site/reading frame used in construct (see methods for criteria). **c)** Three loop insertion sites used for *F5* recombinase site. **d,e)** Primary neurons triple transfected with Cre, Flp, and ChR2-eYFP with or without the indicated insertion site (K75 or L141) expressed eYFP **(d)**, but photocurrents were greatly diminished when reading frame retains the *F5* site **(e)**.

Supplementary Figure 4 - INTRSECT: single-component targeting of cells using multiple-feature Boolean logic

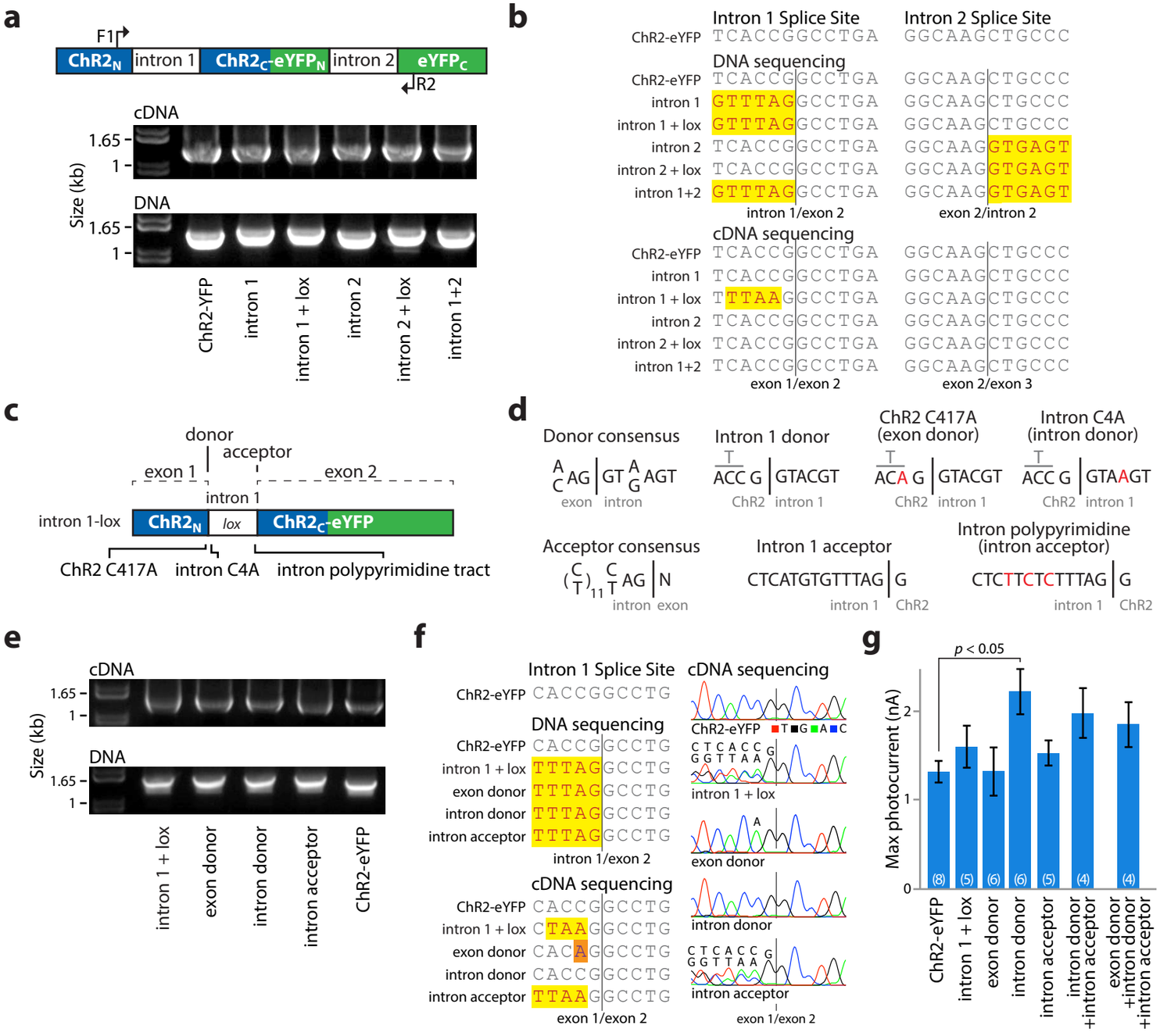

Supplementary Figure 4. Engineering of intron 1 improves splicing fidelity and functional expression of ChR2. a) cDNA prepared from HEK293 cells transfected with indicated constructs and source DNA were amplified by PCR with primers in exons 1 and 3 ('F1/R2'; *top*) and separated by gel electrophoresis (*bottom*). Note that non-spliced DNA bands that contain introns vary in size. **b)** Sequence of DNA isolated from bands in **a**. Yellow background denotes differences from ChR2-eYFP map, representing intron sequence. Intron 1 + lox has mixed sequencing result, suggesting inefficient or mixed splice products. **c)** Schematic of intron 1 position within ChR2-eYFP, donor and acceptor sites, and location of intron modifications. **d)** Consensus, native sequence, and modifications of intron 1 + lox indicated at the single base level. C417A is a silent mutation. **e)** cDNA prepared from HEK293 cells transfected with indicated constructs and source DNA were amplified by PCR and separated by gel electrophoresis. **f)** Sequences of bands from **e** (*left*) with spectrograms (*right*). Note improved splicing efficiency of both exon and intron donor variants compared to native sequence. Mixed sequence was found to represent the correct splice site as well as a product derived from a cryptic splice site 139 bp upstream. Brown background indicates C417A. **g)** Whole cell photocurrents from primary neurons transfected with intron constructs. Photocurrents of ChR2-eYFP containing intron 1 + lox were improved with the consensus intron donor modification (ChR2-eYFP: 1316±120 pA n=8, intron 1 + lox2722: 1603±236 pA n=5, exon donor: 1323±275 pA n=6, intron donor: 2219±258 pA n=6, intron acceptor: 1528.4±1.7 pA n=5, $p<0.05$ Dunnett's multiple comparison tests ChR2-eYFP vs. intron donor).

Supplementary Figure 5 - INTRSECT: single-component targeting of cells using multiple-feature Boolean logic

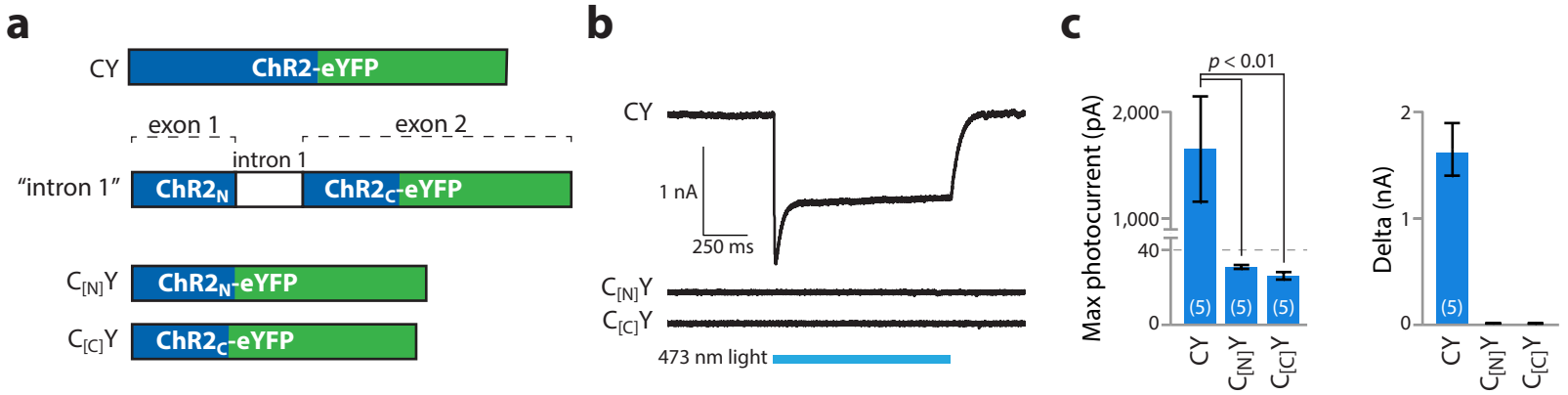

Supplementary Figure 5. ChR2 exons do not encode functional activity in isolation. a) Schematics: ChR2-eYFP without and with an intron, and truncated ChR2 constructs. Note ChR2[N] and ChR2[C] correspond to fragments in exon 1 and exon 2, respectively, in constructs with introns. ChR2[C] has a one-base addition at the 5' terminal to maintain the correct reading frame (construct does not express without this manipulation; data not shown). **b)** Representative whole-cell voltage-clamp recordings from indicated constructs illustrating light response only when the entire ChR2 sequence is present. **c)** Max stimulation photocurrent and delta between baseline and stimulation epochs for ChR2, ChR2[N], and ChR2[C]. One-way type I ANOVA detected significant differences between the maximum photocurrent means ($F_{2,12} = 10.38$, <0.0001); ChR2 group was significantly different from both the N-terminus and C-terminus groups ($p<0.01$ for both, Dunnett's multiple comparison tests). Average change in peak recorded photocurrents from ChR2, ChR2[N], and ChR2[C] were 1614 ± 500 pA , -0.9 ± 2.8 pA, and 5.6 ± 3.0 pA ($n=5$ for each construct).

Supplementary Figure 6 - INTRSECT: single-component targeting of cells using multiple-feature Boolean logic

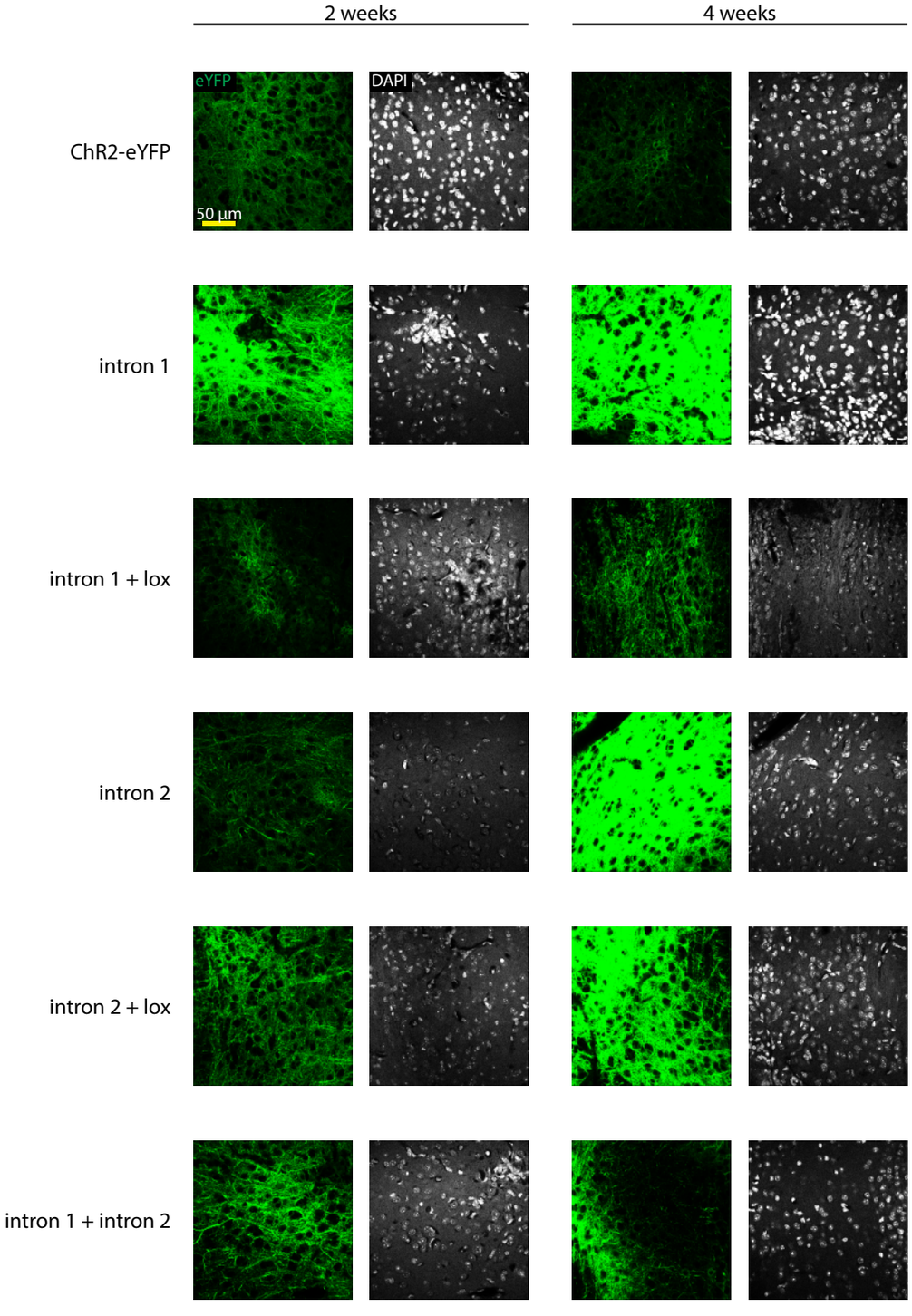

Supplementary Figure 6. ChR2-eYFP is expressed in vivo after addition of introns with or without sequence addition. Lentivirus made from ChR2-eYFP with various intron additions to the reading frame (nomenclature as in Figure 2) driven by human Synapsin promoter was injected into the medial prefrontal cortex of mice bilaterally. Expression was assayed at 2 or 4 weeks after injection. Expression was observed as early as 1 week post-infection (data not shown); all constructs expressed at 2 and 4 week time points, indicating successful intron splicing.

Nature Methods: doi:10.1038/nmeth.2996

Supplementary Figure 7 - INTRSECT: single-component targeting of cells using multiple-feature Boolean logic

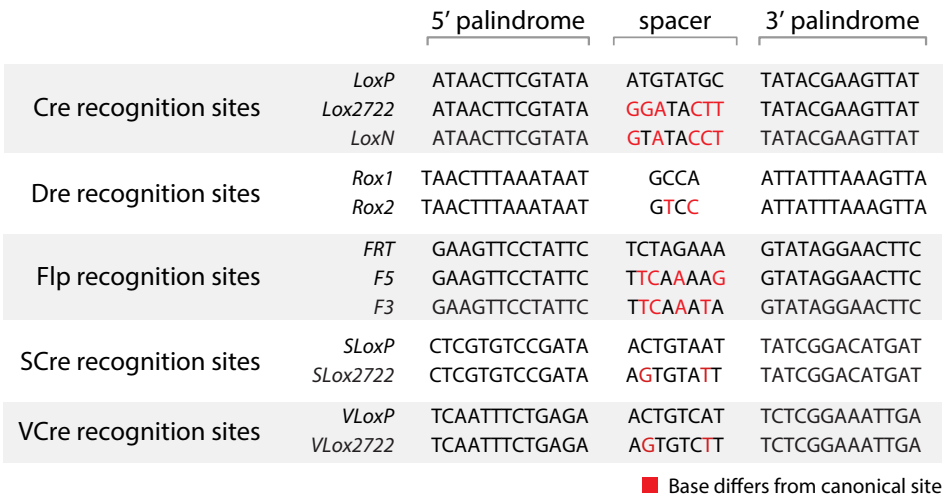

Supplementary Figure 7. Recombinase recognition sites used for integrated intron and recombinase targeting. Recognition site sequences for Cre, Dre, Flp, SCre, and VCre. Red indicates nucleotides that differ from the wild type site.

Nature Methods: doi:10.1038/nmeth.2996

Supplementary Figure 8 - INTRSECT: single-component targeting of cells using multiple-feature Boolean logic

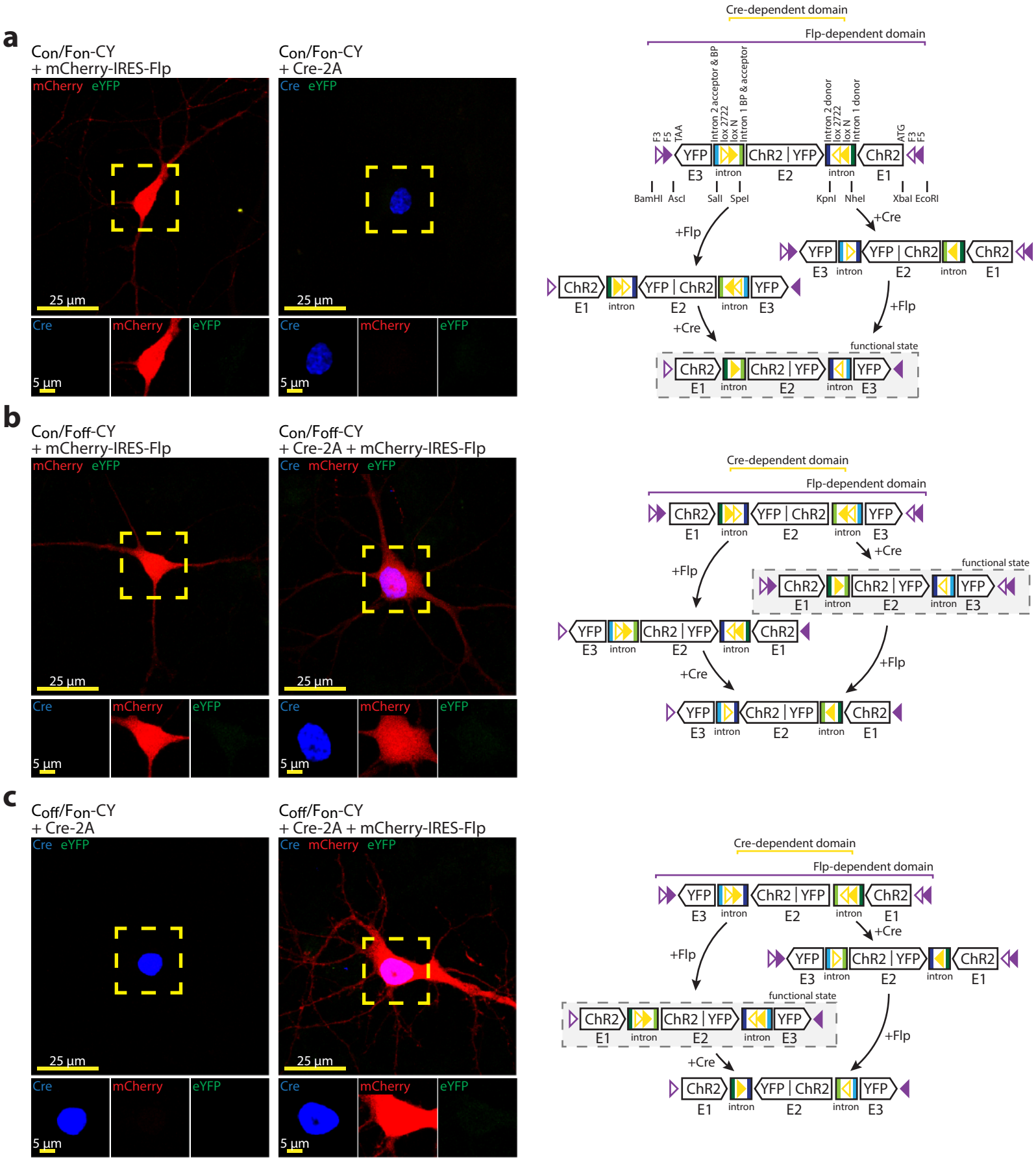

Supplementary Figure 8. Detailed molecular map of integrated intron and recombinase targeting strategies with exemplar non-functional intermediates. ChR2-eYFP in Con/Fon **(a)**, Con/Foff **(b)**, and Coff/Fon **(c)** configurations transfected with Cre (blue) and Flp (red) as indicated (left). No eYFP expression is noted as combinations of recombinases used here do not fulfill the criteria for activation, instead driving ChR2-eYFP to a non-functional configuration (right). For completeness, intronic donor and acceptor sites for both introns as well as all recombinase recognition sites are tracked through each recombinase dependent state. Functional states indicated by dashed box.

Supplementary Figure 9 - INTRSECT: single-component targeting of cells using multiple-feature Boolean logic

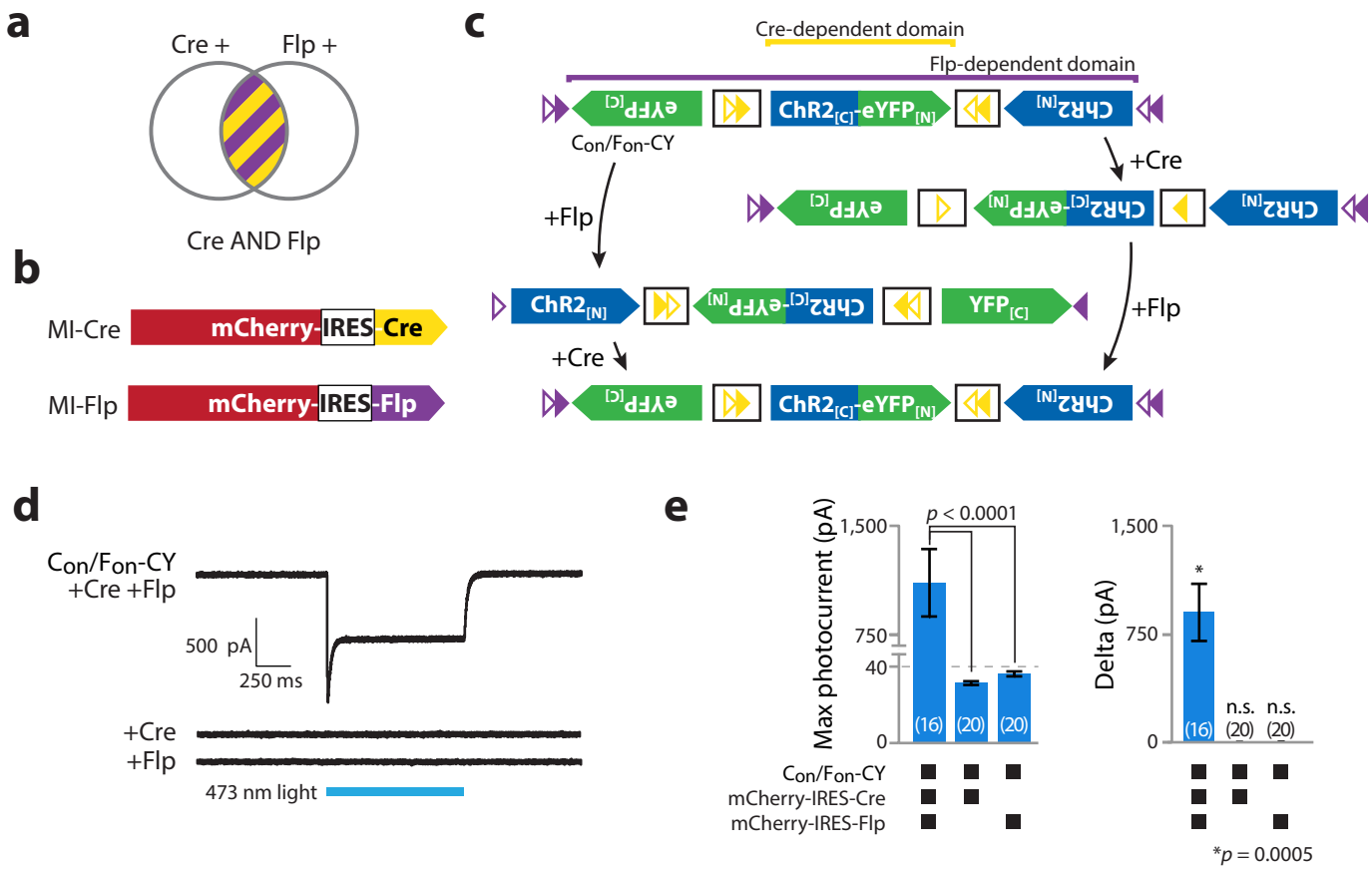

Supplementary Figure 9. Con/Fon-ChR2-eYFP does not generate photocurrents in the absence of either Cre or Flp. **a,b)** Schematic of cells targeted by Con/Fon ChR2-eYFP **(a)** and mCherry-tagged bicistronic constructs **(b)** used for recombinase expression. **c)** ChR2-eYFP is only active after the independent activity of both Cre and Flp recombinase, as no intermediate generated after the isolated activity of a single recombinase generates a coherent open reading frame. **d)** Exemplar voltage clamp recordings from neurons transfected with indicated constructs and patched based only on the expression of mCherry, without examination of eYFP expression. **e)** Max stimulation photocurrent and delta between baseline and stimulation epochs for neurons selected from only mCherry expression. Mean peak photocurrents were 1103.7 ± 235.9 pA for triple transfection (n=16), 27.0 ± 0.8 pA for Cre co-transfection (n=20), and 31.2 ± 1.1 pA for Flp co-transfection (n=20). 14/16 neurons patched in triple transfection condition, 0/20 in Cre only, and 0/20 in Flp only, generated photocurrents more than 2 standard deviations larger than baseline noise. One-way type I ANOVA detected significant differences between the maximum photocurrent means ($F_{2,53} = 26.16$, <0.0001); Con/Fon+MI-Cre+MI-Flp group was significantly different from both the Con/Fon+MI-Cre and Con/Fon+MI-Flp groups during the light-on epoch ($p<0.0001$ for both, Dunnett's multiple comparison tests). Average change in peak recorded photocurrents from +Cre/+Flp, +Cre alone, and +Flp alone were 1071 ± 236 pA , -2.7 ± 1.0 pA, and 1.6 ± 2.4 pA; +Cre/+Flp was significantly different from baseline ($p = 0.0005$, Wilcoxon signed rank t-test).

Supplementary Figure 10 - INTRSECT: single-component targeting of cells using multiple-feature Boolean logic

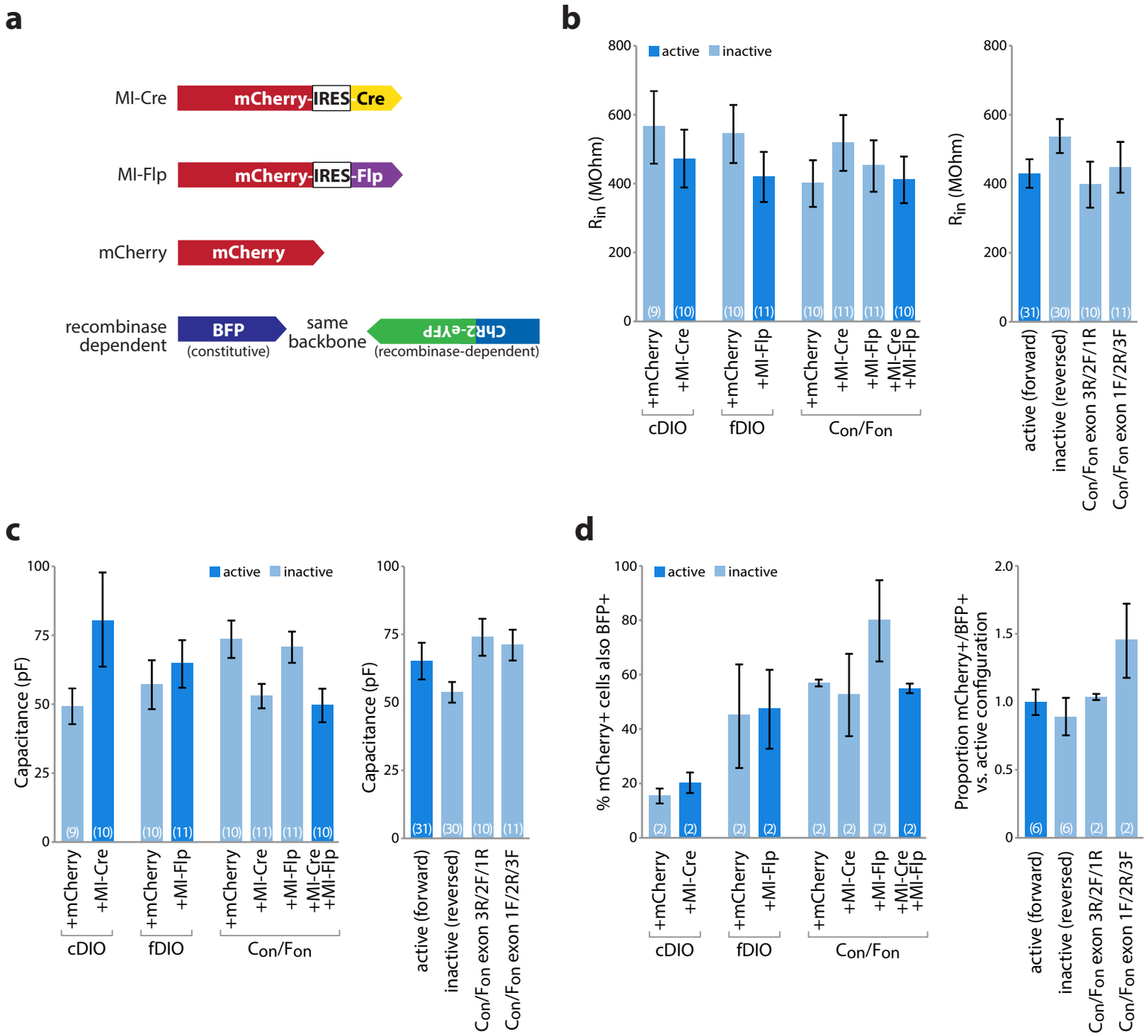

Supplementary Figure 10. Expressing recombinase-dependent constructs in non-active configurations does not influence membrane properties or viability. a) mCherry-tagged recombinases or mCherry were co-transfected with modified variants of fDIO-ChR2-YFP, cDIO-ChR2-eYFP, or Con/Fon-ChR2-eYFP that contain an independently-expressed blue fluorophore to assist in identifying neurons containing non-active recombinase-dependent constructs. **b,c)** No detrimental effect to either **(b)** input resistance or **(c)** capacitance of neurons expressing non-active recombinase-dependent constructs, either grouped by construct (*left*) or by ORF configuration (*right*) was observed. **d)** All recombinase/construct pairings were observed to have similar transfection rates (although an increase in cell number was observed for Con/Fon-ChR2-eYFP+MI-Cre+MI-Flp vs. Con/Fon-ChR2-eYFP+MI-Flp) either grouped by construct (*left*) or ORF configuration (*right*).

Supplementary Figure 11 - INTRSECT: single-component targeting of cells using multiple-feature Boolean logic

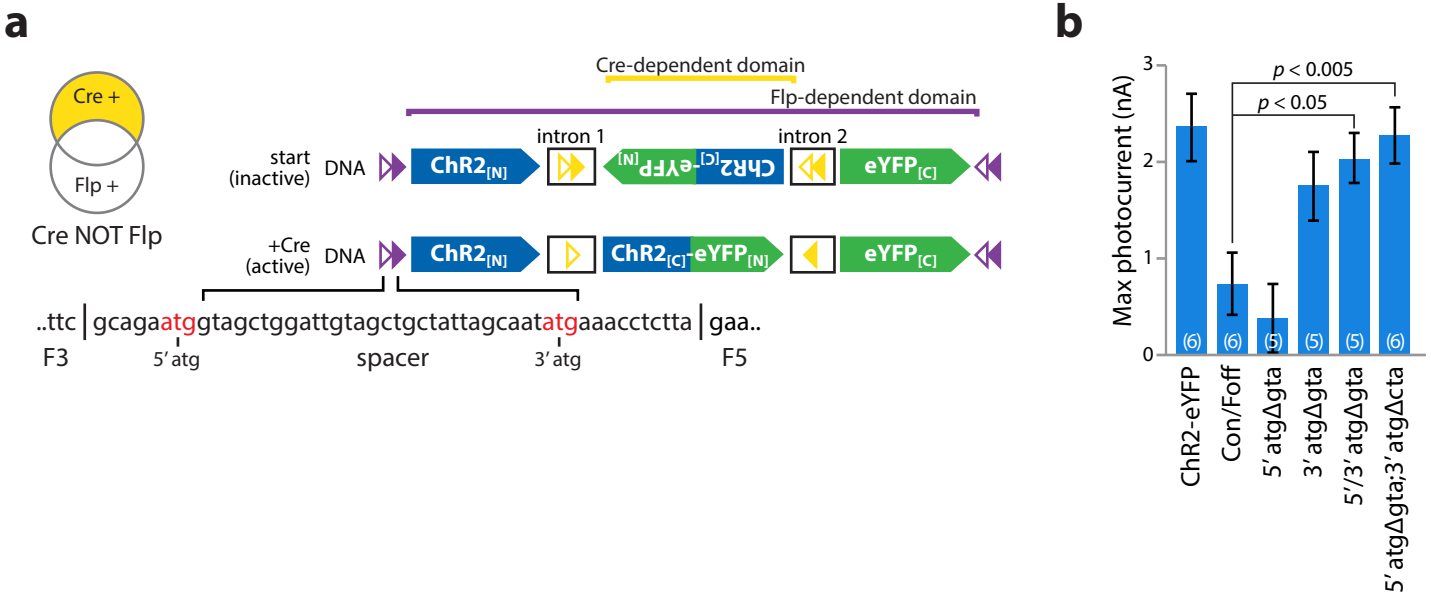

Supplementary Figure 11. Modification of the recombinase recognition sequence spacer region improves functional expression of Con/Foff-ChR2-eYFP. a) Con/Foff-ChR2-eYFP is expressed in neurons that exclusively express Cre recombinase and retains a complete fDIO recombinase recognition cassette in the active configuration, which contains two potential start codons (ATG). **b)** Combined mutations of the 3' and 5' ATG were sufficient to significantly increase photocurrents in Con/Foff-ChR2-eYFP relative to the ATG-containing spacer region (ChR2: 2368.7 ± 348.7 pA n=6, Con/Foff: 735.0 ± 328.1 pA n=6, 5' atgΔgta: 381.0 ± 356.8 pA n=5, 3' atgΔgta: 1758.0 ± 359.0 pA n=5, 5'/3' atgΔgta: 2032.1 ± 260.1 pA n=5, 5' atgΔgta;3' atgΔcta: 2273.6 ± 294.0 pA n=6; $p<0.05$ Bonferroni's Multiple Comparison test $p<0.05$ Con/Foff vs. 5'/3' atgΔgta, $p<0.005$ Con/Foff vs. 5' atgΔgta;3' atgΔcta).

Nature Methods: doi:10.1038/nmeth.2996

Supplementary Figure 12 - INTRSECT: single-component targeting of cells using multiple-feature Boolean logic

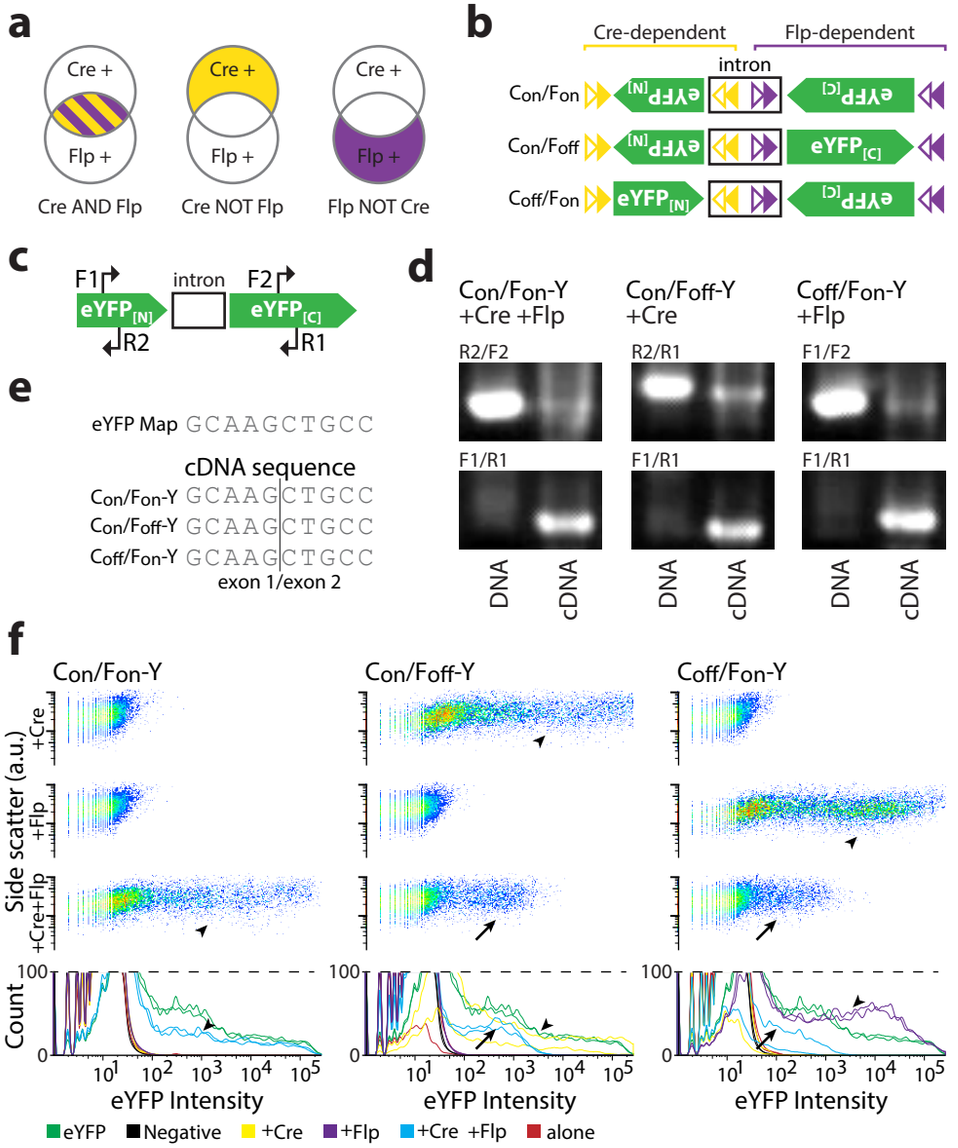

Supplementary Figure 12. INTRSECT approach for intersectional expression of a single ORF with Cre and Flp recombinase. a,b) Schematic of exclusive populations targeted using the combination of one intron with Cre/Flp **(a)** and starting configurations of eYFP exons and recombinase recognition sites **(b)** for Con/Fon (*top*), Con/Foff (*middle*), and Coff/Fon (*bottom*). **c-e)** cDNA was prepared from mRNA of HEK293 cells transfected with indicated constructs. Both the source DNA and cDNA were amplified by PCR with primers **(c)** specific for the starting configuration (**d** *top*) and active, recombinase-dependent configuration (**d** *bottom*) and separated by gel electrophoresis. Primer sets listed above gel images are as in c**.** Bands were excised and sequenced **(e)** and indicated proper splicing in all cases. **f)** Dot exemplar (t*op)* and biological replicate histograms (*bottom*) of flow cytometry analysis of HEK293 cells transfected with indicated constructs and combinations of recombinases indicates specificity in activation (arrowheads) and, in the case of Con/Foff and Coff/Fon that expression levels have decreased 2 or more orders of magnitude after 5 days of expression in culture in the triple transfection (arrows).

Supplementary Figure 13 - INTRSECT: single-component targeting of cells using multiple-feature Boolean logic

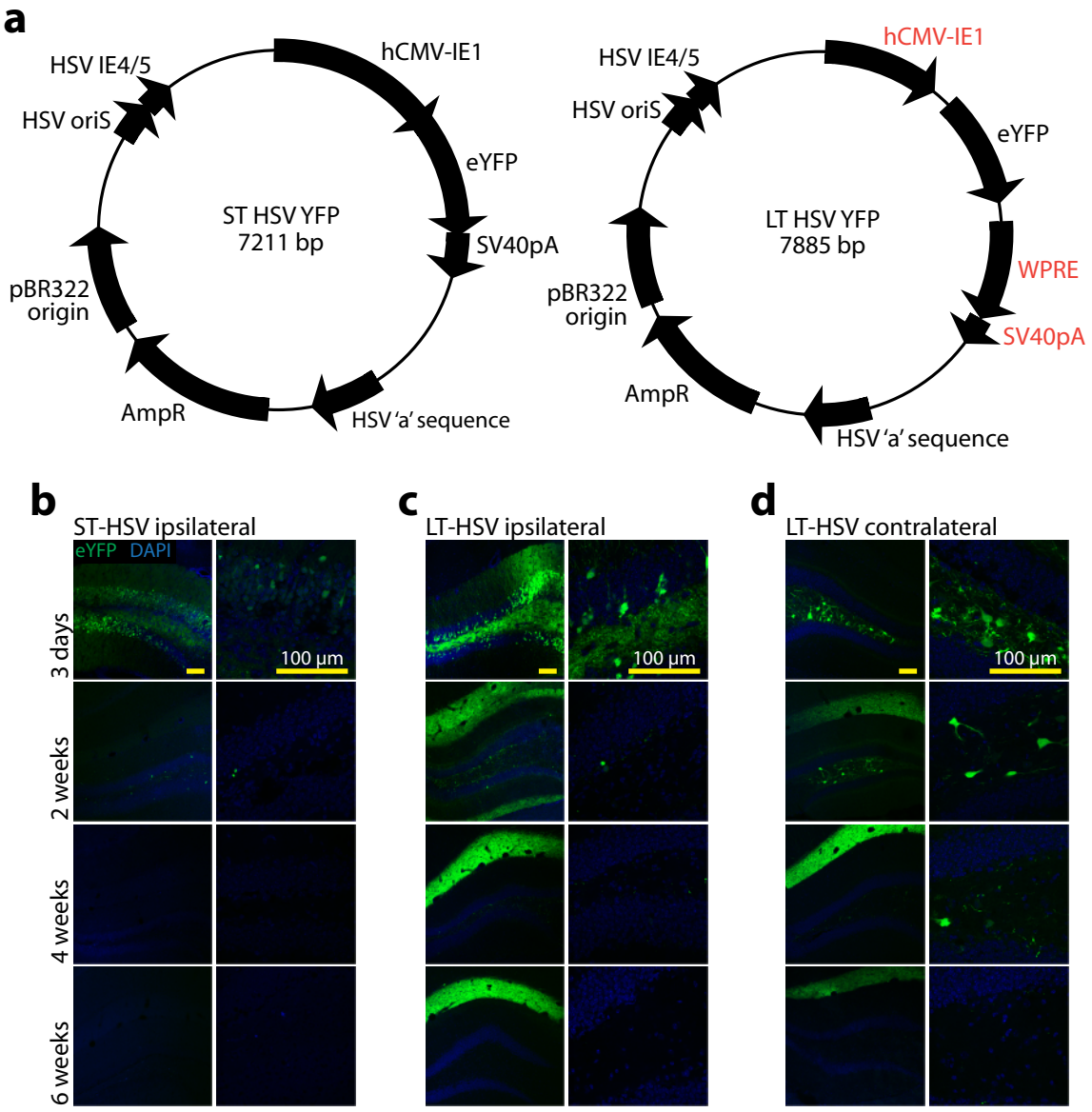

Supplementary Figure 13. In vivo expression time-series and eYFP activation from ST- and LT-HSV. a) Construct maps for ST- and LT-HSV-CMV-eYFP (EF1α promoter in LT-HSV was used for targeting experiments in main figures). **b-d**: Virus (ST- or LT-HSV-CMV-eYFP) was injected unilaterally in dentate gyrus of adult (3-5 month old) mice, and imaged at time-points ranging from 3 days to 6 weeks. Data were obtained from 2 mice for each time-point, with the exception of the later (non-expressing) time-points for ST-HSV, for which only 1 mouse was used per time-point. ST- and LT-HSV were titer-matched (at 3 x 10^8 infectious units per mL) and confocal settings were matched across all conditions. **b)** Virus expression (green) at the injection site for ST-HSV-CMV-eYFP, at low (*left*) and high (*right*) magnification. Cell body expression was seen mainly in the granule cells at the earliest time-point, but disappeared after ~2 weeks. No expression was observed contralaterally at any time-point (data not shown). Cell bodies are labeled by DAPI (blue). **c)** Expression at the injection site for LT-HSV-CMV-eYFP, at low (*left*) and high (*right*) magnification. Cell body expression was seen mainly in the granule cells at the earliest time-point, but disappeared after ~2 weeks. Axonal expression in the molecular layer developed by the 2-week time-point and persisted through 6 weeks. **d)** Expression in the contralateral DG for LT-HSV-CMV-eYFP, at low (*left*) and high (*right*) magnification. Cell body expression was seen mainly in the hilar cells at the earliest time-point, but decreased over time, disappearing by 6 weeks. Axonal expression in the molecular layer developed by the 2-week time-point and persisted through 6 weeks. Confocal settings were matched across all conditions.

Supplementary Figure 14 - INTRSECT: single-component targeting of cells using multiple-feature Boolean logic

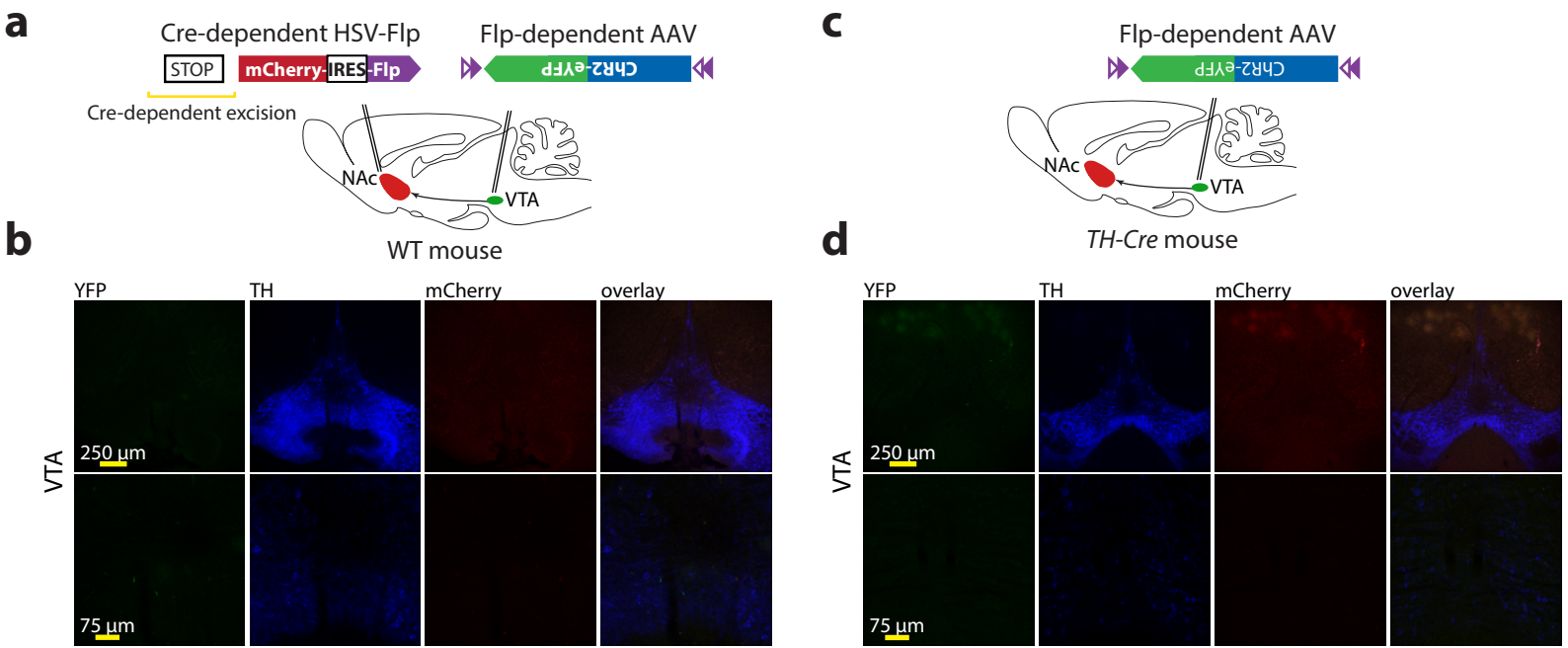

Supplementary Figure 14. Control data for combinatorial targeting with multiplexed recombinases: beyond genetic properties. a) Injection strategy for Cre-negative control. Cre-dependent Flp recombinase packaged in retrograde LT-HSV and Flp-dependent (fDIO) AAV-ChR2-eYFP were injected into the NAcc and VTA of a wild type mouse, respectively. **b)** *In vivo* expression pattern in the VTA, showing no eYFP expression as expected. **c)** Injection strategy for Flp-negative control. A Flp-dependent (fDIO) AAV-ChR2-eYFP was injected into the VTA of a *TH-IRES-Cre* mouse. **d)** *In vivo* expression pattern in the VTA, showing minimal eYFP expression.

Nature Methods: doi:10.1038/nmeth.2996

Supplementary Figure 15 - INTRSECT: single-component targeting of cells using multiple-feature Boolean logic

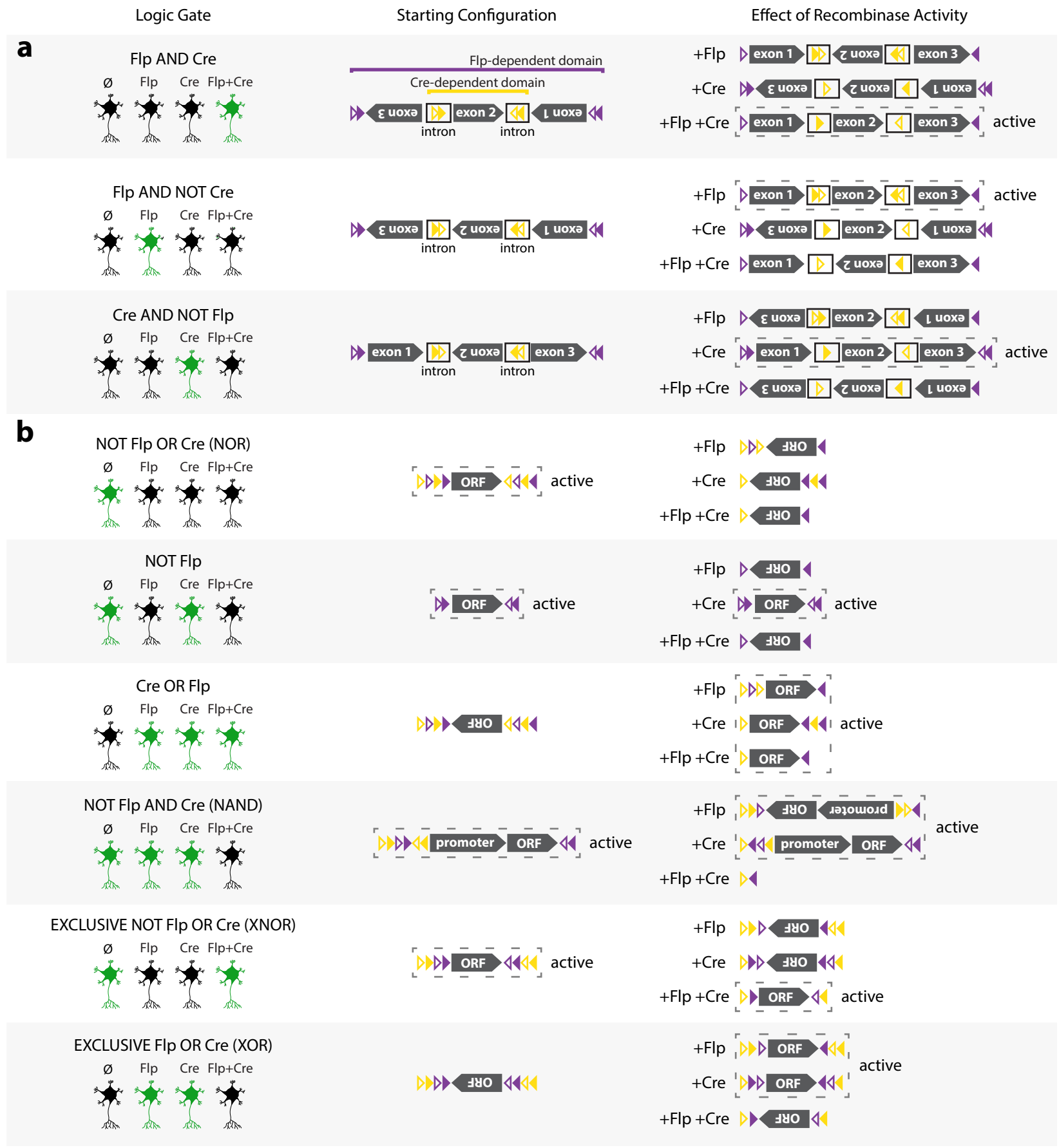

Supplementary Figure 15. Diversity of INTRSECT-based logical operations. In addition to targeting cells that express a single recombinase exclusively or only cells expressing two recombinases (**a**; green cells), Cre and Flp may be used together to achieve additional expression patterns (**b**; 'Logic Gate') by changing the initial relative configuration/position of the ORF and recombinase recognition sites ('Starting Configuration') to direct response of the construct in response to recombinases ('Effects of Recombinase Activity'). Active configurations denoted by dashed boxes. Note that NOR may also be achieved using intron-based multiple recombinase configuration.

Nature Methods: doi:10.1038/nmeth.2996

Supplementary Figure 16 - INTRSECT: single-component targeting of cells using multiple-feature Boolean logic

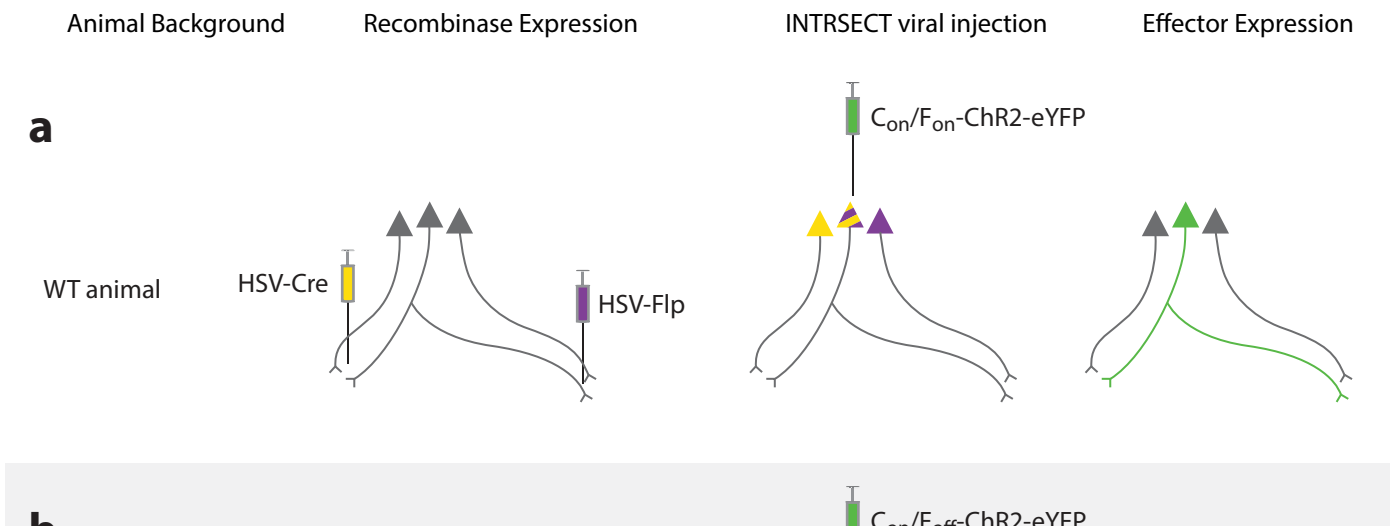

Supplementary Figure 16. Combinatorial INTRSECT approaches. These multiple recombinase-dependent constructs may be combined with retrograde viral delivery of recombinases to target cells based on multiple traits. **a,b)** Viral delivery of Cre and Flp may be achieved using HSV tools described in this manuscript and may be combined with upstream delivery of AAV-DJ-Con/Foff-ChR2-eYFP in order to specifically express a genetic tool within neurons with collateralized projections **(a)** or to exclude a population of neurons projecting to multiple defined downstream locations **(b)**. **c)** Transgenic animals expressing Cre within a defined locus are able to extend targeting control to include cells that both project to multiple defined loci AND have a specified genetic background. **d)** Last, a palette of injected viruses may be used to elucidate the expression patterns of multiple neuron subtypes using simultaneous injection of both AND as well as NOT conditional viruses controlling expression of various fluorophores.

Nature Methods: doi:10.1038/nmeth.2996